

## Determination of the Corrosion Resistance of SS-304 in Synthetic Seawater at Two Temperatures Using Electrochemical Noise and Polarization Curves

Diego Mendoza Morales, Cecilia Cuevas Arteaga \*

Research Center in Engineering and Applied Sciences, Autonomous University of the Morelos State, Av. Universidad 1001, Col. Chamilpa, Cuernavaca, Mor., Mexico, C.P. 62209.

\*E-mail: [ccuevas@uaem.mx](mailto:ccuevas@uaem.mx)

Received: 13 June 2016 / Accepted: 5 August 2016 / Published: 6 September 2016

---

In this paper two electrochemical techniques were used to study the behavior of Stainless Steel 304 in synthetic seawater. The synthetic seawater was elaborated according to the standard ASTM D 1141-98 (Standard Practice for the preparation of substitute ocean water). Two different temperatures were used in the experiments: room temperature and 40 °C. The electrochemical techniques were potentiodynamic polarization curves and electrochemical noise. The electrochemical noise was analyzed in the time domain and in the frequency domain, the noise resistance ( $R_n$ ) and the spectral noise resistance ( $R_{sn}^0$ ) were obtained. The corrosion rate at 40 °C was higher than the corrosion rate at room temperature, but the values of noise resistance and spectral noise resistance were high at both temperatures, indicating the good resistance of the chromium oxide layer to the increment of temperature.

---

**Keywords:** Stainless Steel 304, Synthetic Seawater, electrochemical noise, potentiodynamic polarization curves.

### 1. INTRODUCTION

The electronic structure of the passive films formed on stainless steels materials can be described by a bilayer model composed of an outer layer of iron oxide ( $Fe_2O_2$ ) and hydroxides, which are near the solution; and an inner layer made of chromium oxide ( $Cr_2O_3$ ) covering the metal surface [1-2]. The bilayer model has been used to describe the semiconducting properties of the metallic oxides formed in Fe-Cr alloys exposed to sulfuric acid solutions, assuming that these passive layers were composed of an outer layer made of hydroxides of chromium III ( $Cr[OH]_3$ ), and an inner layer made of chromium oxide ( $Cr_2O_3$ ) [2-3].

However, the bilayer structure formed on the stainless steels materials has proved to be even more complex [4-6]. The outer layer would be enriched with  $\text{Fe}^{3+}$  species such as  $\text{Fe}_2\text{O}_3$ , ferrous oxy-hydroxides ( $\text{FeO}[\text{OH}]$ ) and hydroxides of iron III ( $\text{Fe}[\text{OH}]_3$ ), this region could also have  $\text{Cr}(\text{OH})_3$  and chromium oxy-hydroxides ( $\text{CrO}[\text{OH}]$ ). The inner layer consists of a combined mixture of iron oxides and chromium, the more exact formula to represent this combination would be  $\text{Fe}(\text{II})[\text{Cr}(\text{III})_x\text{Fe}(\text{III})_{(1-x)}]_2\text{O}_4$ , where  $0 < x \leq 1$ . There could also be nickel replacing the iron or chromium in the crystalline structure [4-6].

The thickness of the passive oxide layers formed on stainless steels materials varies from 1 to 3 nm (10 to 30 Å). Such as it is expected, high temperatures and acidic environments tend to decrease the thickness of these layers [7]. The passive layers can be amorphous, nanocrystalline or crystalline [8-10]. To study the effect of the progressive addition of chromium into the iron, Mc Bee and Kruger used electron diffraction and proved that the passive layers change from a polycrystalline state to an amorphous state by increasing the amount of chromium in the alloy [11].

In view of these observations, it is proposed that one of the most important factors in the passivity of metals is the structure of the passive layer [12]. It is believed that an amorphous oxide provides more protection against corrosion than a crystalline one, since the crystalline structures present grain boundaries and have some defects that may help the migration of metal cations to the solution. Stainless steels materials contain a minimum of 11% chromium, which causes the formation of an adherent and compact chromium oxide, protecting the stainless steels from corrosion. The effects of adding various elements to an alloy have been studied over the years, therefore the following effects have been observed in the passivation [13]:

- a) Chromium is beneficial to iron and nickel, but it is not beneficial to molybdenum.
- b) Molybdenum is not beneficial to iron and nickel, however it is beneficial to Fe-Cr alloys and Fe-Cr-Ni alloys.
- c) Nickel is beneficial to iron and molybdenum, but it is not beneficial to chromium.

The stainless steel mostly used around the world is the stainless steel 304 (SS-304), the standard chemical composition of this steel is shown in Table 1. The SS-304 has a good corrosion resistance, however presents localized corrosion in the presence of chloride and bromide ions [14-16]. This fact has limited the use of SS-304 in seawater applications. The susceptibility to localized corrosion in stainless steels is measured by using the pitting resistance equivalent number (PREN) [17-18]:

$$\text{PREN} = \% \text{Cr} + 3.2\% \text{Mo} + 16\% \text{N} \quad (1)$$

It is said that PREN must have a minimum value of 38 to prevent pitting, the PREN of SS-304 is approximately 20 and therefore this steel can suffer pitting corrosion, nevertheless, in general the resistance of SS-304 to uniform corrosion is excellent [17-18]. The addition of molybdenum and nitrogen to the stainless steels is desirable to increase the resistance to pitting corrosion. The aim of this research is to evaluate the corrosion performance of SS-304 in seawater at two temperatures using two electrochemical techniques: potentiodynamic polarization curves (PP) and electrochemical noise (EN), making a comparison of the results.

**Table 1.** Standard chemical composition of SS-304

Element	% in Weight
Carbon	.08 max.
Manganese	2 max.
Phosphorus	.045 max.
Sulfur	.03 max.
Silicon	.75 max.
Chromium	18-20
Nickel	8.0-12
Nitrogen	0.1 max.
Iron	Balance

## 2. EXPERIMENTAL PROCEDURES

A rod of SS-304 was cut to obtain small parallelepiped samples of  $10 \times 10 \times 3 \text{ mm}^3$ , a copper wire was welded to these samples, and then the samples were encapsulated in epoxy resin. In all the experiments the area of the exposed metal was  $1 \text{ cm}^2$ . The samples were abraded with wet SiC paper, the initial grit size was 120 and the final one was 600. Finally, the samples were cleaned with an ultrasonic bath and dried in a stream air.

The synthetic seawater was prepared in accordance with ASTM D 1141-98 (Standard Practice for the preparation of substitute ocean water), using only analytical grade reagents [19]. Table 2 shows the composition of the synthetic seawater, the pH was adjusted to a value of 8.2 using a solution of 0.1 M NaOH. The chlorinity of this seawater was 19.38 [19]. The electrochemical tests were conducted at two different temperatures: the room temperature and  $40 \text{ }^\circ\text{C}$ . The reference electrode was a Thermo Scientific Orion Cat. No. 900100, the electrochemical potential of this reference electrode is equivalent to the potential of a saturated calomel electrode (SCE). In order to perform the electrochemical tests, an Interface 1000 (Potentiostat/Galvanostat/ZRA) of Gamry Instruments was used in all the experiments.

**Table 2.** Chemical composition of the synthetic seawater.

Compound	Concentration (g/L)
NaCl	24.53
MgCl <sub>2</sub>	5.2
Na <sub>2</sub> SO <sub>4</sub>	4.09
CaCl <sub>2</sub>	1.16
KCl	0.695
NaHCO <sub>3</sub>	0.201
KBr	0.101
H <sub>3</sub> BO <sub>3</sub>	0.027
SrCl <sub>2</sub>	0.025
NaF	0.003

The electrochemical cell employed in the noise tests consisted of two working electrodes and the reference electrode previously mentioned, the working electrodes are the samples of SS-304 encapsulated in the epoxy resin, the three electrodes were immersed in the synthetic seawater.

The electrochemical cell was used to measure the current and the voltage noise simultaneously, connecting the cell to the ZRA (zero resistance ammeter). In ZRA tests, the current is measured between the two working electrodes which are held at the same potential (a short circuit between the electrodes), the voltage is measured independently between the two specimens and the reference electrode [20].

The electrochemical noise tests lasted 10 days and the measurements were taken every 6 hours, each measurement consisted of 2048 points obtained with a sample rate of 2 points/second, then each time series lasted 1024 s.

The experimental arrangement used in the potentiodynamic polarization curves was similar to the arrangement used in electrochemical noise tests, but a platinum counter electrode was used in place of one of the two working electrodes. The potentiodynamic polarization curves (PP) were done after 30 minutes of exposing the SS-304 in the synthetic seawater, the applied over-potential was -120 mV to 1500 mV with respect to open circuit potential, with a scan rate of 1 mV/s.

At the end of the 10 days of immersion, the corroded surface of the samples was analyzed using a scanning electron microscope (SEM), model LEO 1450 VP equipped with an EDS (Energy Dispersive Spectrometer) of X-rays.

### 3. RESULTS AND DISCUSSION

#### 3.1. Physical Characterization

Two images obtained with the SEM are presented in figures 1.a and 1.c, the images of SS-304 at both temperatures did not show evidence of localized corrosion. It is possible that 10 days of immersion in the synthetic seawater is a short time in order to observe pitting corrosion. In this work only the images of the samples at 40 °C are presented, where the presence of corrosion products was evident, see Figures 1.a and 1.c. Even though the samples at room temperature also presented some corrosion products, but in much less extension.

The semi-quantitative chemical composition in weight percentage of the corrosion products is shown at the right side of each corroded sample, see Figures 1.b and 1.d. The corrosion products clearly show the presence of oxygen, iron, chromium and traces of nickel, these elements are present in the composition of the stainless steel. There is also the presence of chlorine, sodium and magnesium, which are constituents of the synthetic seawater. The large amount of chlorine and sodium suggests the possibility of a thin layer of sodium chloride covering the metal oxide.

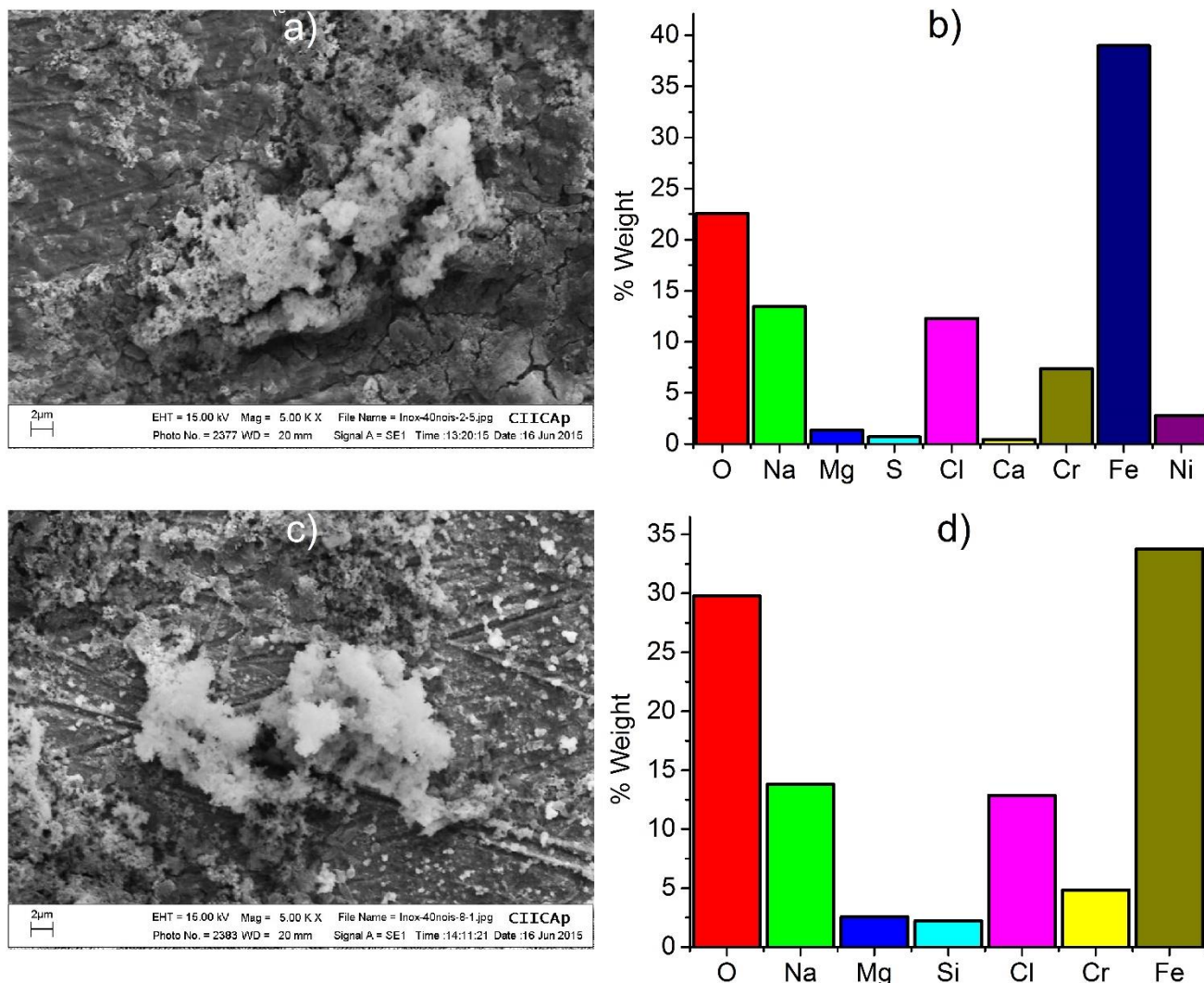


**Figure 1.** Images obtained with the SEM at 40 °C in the noise test samples. a) and c) Images showing corrosion products, b) and d) Semi-quantitative chemical composition in weight percentage obtained with the EDS (Energy Dispersive Spectrometer) of X-rays, b) and d) corresponds to a) and c) respectively.

The SEM detects better the outermost surface of a material, which presumably contains iron hydroxides for the SS-304, and this is a probable explanation for the small amount of chromium and nickel in the semi-quantitative analysis. The calcium and magnesium in Figure 1 can indicate the presence of  $\text{CaCO}_3$  and  $\text{Mg}(\text{OH})_2$  in the corrosion products, this two compounds tend to precipitate at high values of pH, and they are benefic to reduce the corrosion rate in the cathodic protection of marine structures [21].

### 3.2. Potentiodynamic Polarization Curves

Figure 2 shows the polarization curves of SS-304 obtained at room temperature and at 40 °C. The corrosion potential at room temperature was -221.34 mV vs. SCE, and at 40 °C it was -240.8 mV vs. SCE. Contrary to what was expected, the presence of a passive region was not observed in the

polarization curves. At 40 °C a clear increase in the anodic oxidation is observed above 50 mV vs. SCE, where the current density increased from 0.003 mA/cm<sup>2</sup> to 1 mA/cm<sup>2</sup>, this behavior probably states the pitting potential at 40 °C [22]. It can be seen an asymptotic trend in the current density at high anodic overpotentials, which is due to the diffusive effects in the metal-electrolyte interface. These effects hinder the transport of Fe<sup>2+</sup> ions into the solution, which had been previously saturated with such ions.

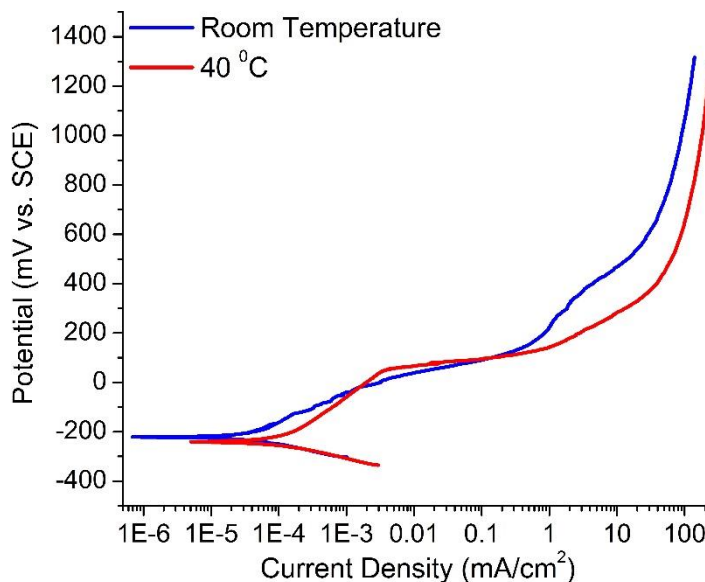


**Figure 2.** Potentiodynamic Polarization Curves of SS-304 in the synthetic seawater at room temperature and at 40 °C.

Tafel slopes and the corrosion rate were determined using the Tafel extrapolation method. For the experiment at room temperature, the corrosion rate is 4.0x10<sup>-5</sup> mA/cm<sup>2</sup>, the anodic and cathodic Tafel slopes are 145.45 mV/decade and 62.54 mV/decade respectively. For the experiment at 40 °C the corrosion rate is 8.91x10<sup>-5</sup> mA/cm<sup>2</sup>, and the anodic and cathodic Tafel slopes are 156.50 mV/decade and 64.95 mV/decade respectively. In this case the corrosion rate at 40 °C is higher than that at room temperature. It is also seen that the corrosion potential at room temperature is nobler than that at the higher temperature.

In both cases the Tafel slopes are very similar and no significant changes are worth to comment. The Stern and Geary equation can be used to calculate the corrosion rate, but also to obtain the polarization resistance such as shown in equation 2 [23-24].

$$R_p = \frac{B}{i_{corr}} = \frac{b_a b_c}{2.303(b_a + b_c)} * \frac{1}{i_{corr}} \tag{2}$$

Where R<sub>p</sub> is the linear polarization resistance in ohms.cm<sup>2</sup>, i<sub>corr</sub> is the corrosion rate in mA/cm<sup>2</sup>, b<sub>a</sub> and b<sub>c</sub> are the anodic and cathodic Tafel slopes respectively in mV/decade. At 40 °C the R<sub>p</sub> was

223,538.85 ohm.cm<sup>2</sup> and at room temperature the  $R_p$  was 474,760 ohm.cm<sup>2</sup>, being the  $R_p$  at 40 °C smaller than that at room temperature.

### 3.3. Electrochemical Noise Tests

Figure 3 shows the potential and current noise records corresponding to the ambient temperature, also Figure 4 shows the potential and current noise records corresponding to 40 °C. Day 0 in Figures 3 and 4 corresponds to the beginning of the experiment, Day 5 is the middle of the experiment and Day 10 is the end of the experiment. From the potential noise records at both temperatures, we could see that the electrochemical potential tended to become nobler with time, indicating an improvement of the passive layer to protect the metal. During the experiments, the electrochemical potentials at both temperatures were in an interval from -280 to 42 mV vs. SCE, the nobler values were reached in the 10 Day by the samples maintained at room temperature (Figure 3.e).

The values of current noise were very low in the order of nanoamperes, indicating a very high impedance of the SS-304 in the synthetic seawater, the only exception to this behavior is the current noise record corresponding to Day 0 at 40 °C (Figure 4.b), this noise record shows a transient that reached almost the -1000 nA/cm<sup>2</sup>, this transient could indicate the presence of a metastable pit, but the posterior analysis in SEM didn't show the presence of pitting corrosion, the other peaks or possible transients in the other current noise records were extremely low to cause a pit in the metal surface. A very important factor that promotes the growing of a pit is the acidity of the solution inside the pit [13], the pH of the seawater was 8.2 and this basic pH in combination with the high impedance of the system stopped the formation of pits.

Figure 5 shows the current and potential noise records obtained after 6 hours of immersion at room temperature, figures 5.a and 5.b show a current noise record and a potential noise record respectively. Figures 5.c and 5.d show the same records after subtracting the linear trend, the linear trend was removed in all the noise records [25-28]. To remove the linear trend was necessary to fit a straight line by the method of least squares (regression analysis), see the red lines in Figures 5.a and 5.b. After removing the linear trend, the noise resistance ( $R_n$ ) was determined,  $R_n$  is equal to the standard deviation of the potential noise divided by the standard deviation of the current noise [26].

The Current and Potential Power Spectral Densities ( $\Psi_I$  and  $\Psi_V$ ) were calculated after the elimination of the linear trend, see Figures 5.e and 5.f. The Power Spectral Density (PSD) is the power (or variance) present in a signal as a function of the frequency, which is a density because the power is divided by the width of the frequency band, so the units of  $\Psi_V$  and  $\Psi_I$  are V<sup>2</sup>/Hz and A<sup>2</sup>/Hz respectively. There are two methods commonly used in corrosion science to calculate the PSD: The Fourier Transform and the Maximum Entropy Method [29, 30].

In this paper, the Discrete Fourier Transform is used to calculate  $\Psi_I$  and  $\Psi_V$ . The Discrete Fourier Transform converts  $M$  values of a time record into  $M/2$  values of PSD. The PSD uses a frequency range from  $1/T$  to  $1/2\Delta t$  (Nyquist Frequency) [20, 31].  $T$  is the data acquisition time and  $\Delta t$  is the sampling time interval, for the noise records presented in this article:  $M = 2048$ ,  $T = 1024$  s and  $\Delta t = 0.5$  s. Equation 3 is used to calculate the Discrete Fourier Transform ( $X_T$ ) of a digitalized noise

signal  $x(n\Delta t)$  in which  $n$  is an integer number whose value ranges from 0 to  $M-1$ ,  $m\Delta f$  is the frequency at which the Fourier Transform is calculated and  $m$  is an integer number whose value ranges from 1 to  $M/2$ . For the Power Spectral Densities presented in this paper, the frequency interval was  $0.9766 \text{ mHz} \leq m\Delta f \leq 1 \text{ Hz}$ , because  $\Delta f = 1/M\Delta t = 1/T = 0.9766 \text{ mHz}$  [31].

Equation 4 shows how to calculate the PSD from the Fourier transform previously calculated with Equation 3 [31]. Nowadays the Discrete Fourier Transform is calculated using a powerful computer algorithm known as the Fast Fourier transform (FFT).

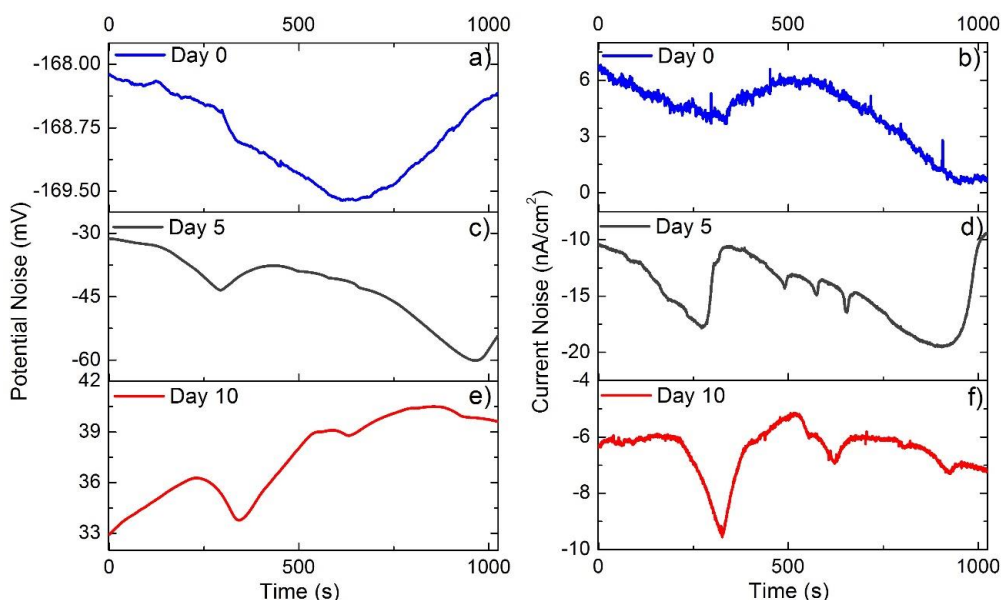


**Figure 3.** Noise records corresponding at room temperature. a) potential noise in day 0, b) current noise in day 0, c) potential noise in day 5, d) current noise in day 5, e) potential noise in day 10, f) current noise in day 10.

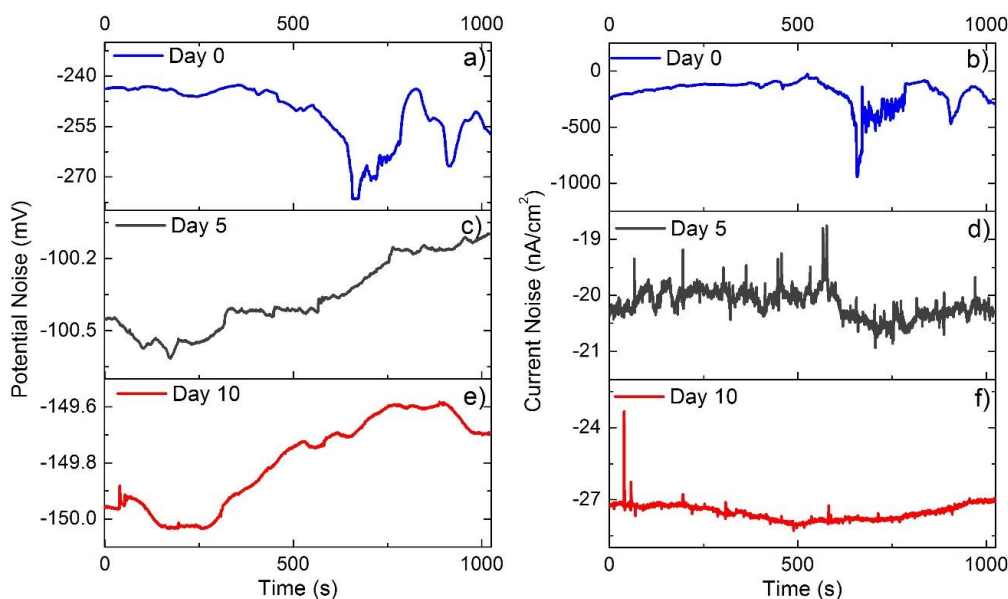


**Figure 4.** Noise records corresponding to 40 °C. a) potential noise in day 0, b) current noise in day 0, c) potential noise in day 5, d) current noise in day 5, e) potential noise in day 10, f) current noise in day 10.

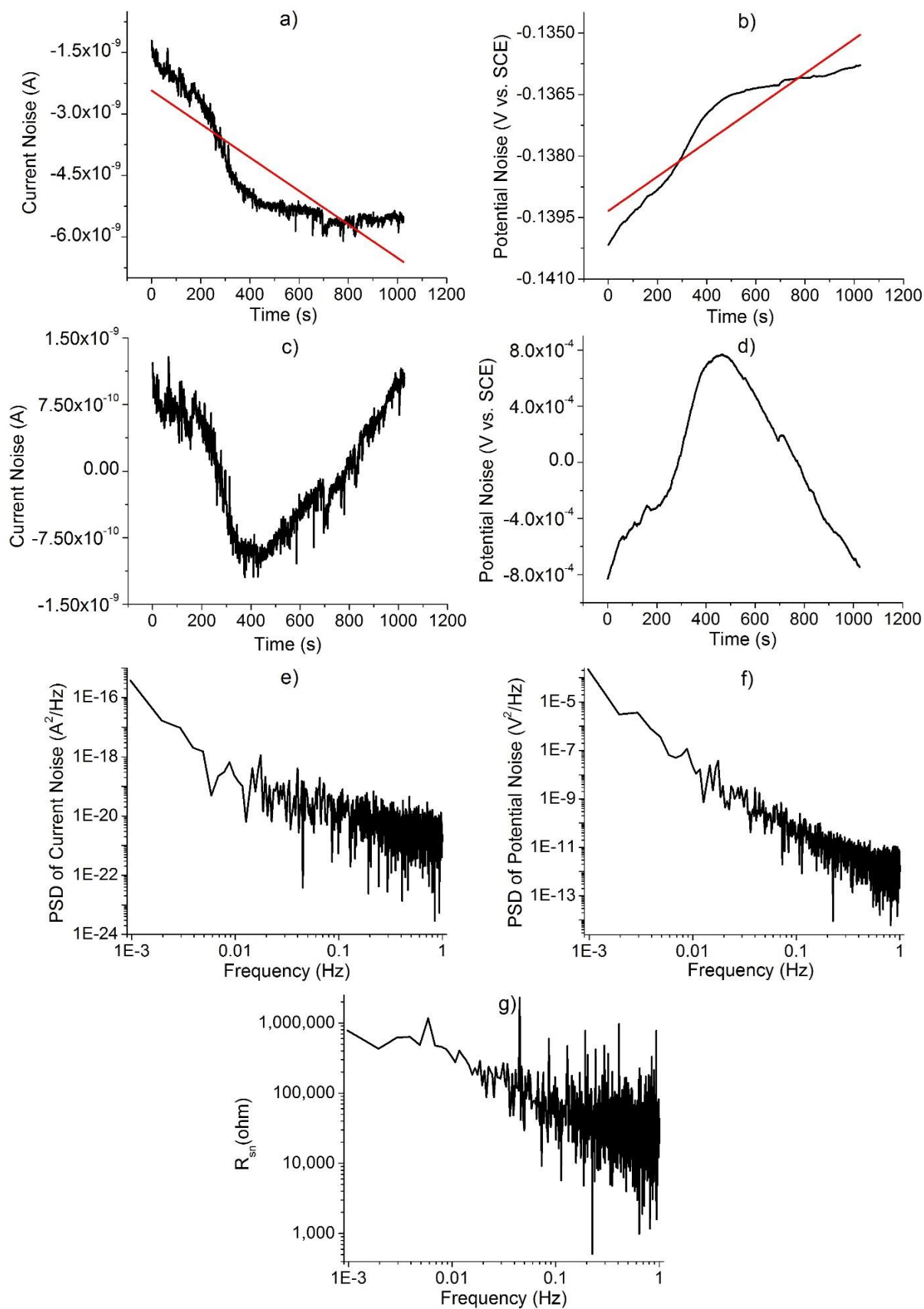


**Figure 5.** Step by step procedure to obtain  $R_{sn}(f)$ . a) Current Noise, b) Potential Noise, c) Current Noise without linear trend, d) Potential Noise without linear trend, e) PSD of Current Noise, f) PSD of Potential Noise, g) Spectral Noise Response.

$$X_T(m\Delta f) = \sum_{n=0}^{M-1} x(n\Delta t) * \exp[-2j\pi(m\Delta f)(n\Delta t)] * \Delta t \quad (3)$$

$$\Psi_x(m\Delta f) = \frac{2}{T} |X_T(m\Delta f)|^2 \quad (4)$$

A free program developed by F. Huet was used to calculate the Power Spectral Densities [32]. The spectral noise response “ $R_{sn}(f)$ ” can be calculated using the Fourier Transform of potential and current ( $V_T$  and  $I_T$ ) or by using the Power Spectral Densities of potential and current ( $\Psi_V$  and  $\Psi_I$ ), see Equation 5 [25, 31, 33-35]. The  $R_{sn}(f)$  comprises an interval of frequencies from  $1/T$  to  $1/2\Delta t$  (Nyquist Frequency). Figure 5.g shows the spectral noise response obtained with the data of Figures 5.e and 5.f.

$$R_{sn}(f) = \frac{|V_T(f)|}{|I_T(f)|} = \sqrt{\frac{\Psi_V(f)}{\Psi_I(f)}} \quad (5)$$

$R_{sn}(f)$  represents an estimation of the magnitude of the electrochemical impedance, so the data of  $R_{sn}(f)$  can be compared with the data obtained with the Electrochemical Impedance Spectroscopy (EIS) [36, 37], but  $R_{sn}(f)$  has some limitations with respect to the EIS technique. For example, the maximum frequency of  $R_{sn}(f)$  is equal to the Nyquist Frequency, and  $\Delta t$  must be equal to  $5 \times 10^{-6}$  s to achieve a maximum frequency of 100,000 Hz, this  $\Delta t$  is extremely low, and most of the potentiostats are not capable to apply.

Another important limitation with  $R_{sn}(f)$  is the total loss of the phase data, so  $R_{sn}(f)$  cannot be compared with the Bode Phase Plots in anyway. The Spectral Noise Resistance “ $R_{sn}^0$ ” is the low frequency limit of  $R_{sn}(f)$ , see equation 6. Many times the DC limit is not clear, so  $R_{sn}^0$  is determined as the average of the 5 or 10 data points located in the region of lowest frequency [38-39].

$$R_{sn}^0 = \lim_{f \rightarrow 0} R_{sn}(f) \quad (6)$$

There has been observed for iron in various corrosive environments a good agreement between  $R_n$  and  $R_{sn}^0$ . Figure 6 shows the evolution of the noise resistance and the Spectral Noise Resistance at the two temperatures. The average value of  $R_n$  at room temperature was 1,492,645 ohm.cm<sup>2</sup> and the average value of  $R_n$  at 40 °C was 315,658 ohm.cm<sup>2</sup>. The average value of  $R_{sn}^0$  at room temperature was 1,671,624 ohm.cm<sup>2</sup> and the average value of  $R_{sn}^0$  at 40 °C was 403,259 ohm.cm<sup>2</sup>. There is a slight upward trend in the values of  $R_n$  and  $R_{sn}^0$  obtained at 40 °C, indicating an improvement in the protection against corrosion.

It can be seen from Figure 6 that the values of  $R_n$  and  $R_{sn}^0$  are always greater at room temperature than those values at 40 °C. The average value of  $R_{sn}^0$  at a given temperature is greater than the average value of  $R_n$  at the same temperature, this is expected because  $R_{sn}^0$  is the limit of the magnitude when the frequency tends to zero and therefore  $R_{sn}^0$  should be higher than  $R_n$ .

Equation 7 shows the mathematical relationship to calculate the localization index (LI). This parameter can be used as an indicator to determine if the corrosion process is uniform or localized. LI is equal to the standard deviation of the current noise “ $S_I$ ” divided by the root mean square of current noise “rms(I)”. LI cannot be greater than 1, a value below 0.01 indicates uniform corrosion, a value from 0.01 to 0.1 indicates mixed corrosion and a value from 0.1 to 1 indicates localized corrosion [40-41].

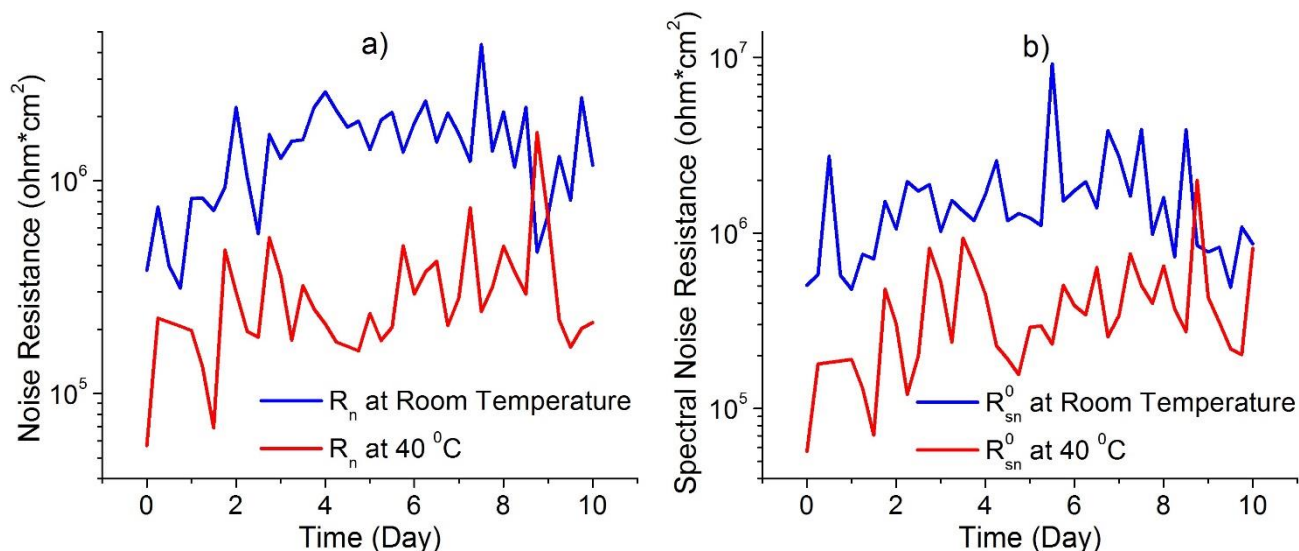


**Figure 6.** Noise Resistance ( $R_n$ ) and Spectral Noise Resistance ( $R_{sn}^0$ ) at room Temperature and at 40 °C. a)  $R_n$ , b)  $R_{sn}^0$ .

$$LI = \frac{S_I}{rms(I)} \tag{7}$$

LI is calculated before removing the linear trend in the current noise records, if LI were calculated after the removing, then LI would be always equal to 1. LI has received some observations, since two electrodes having identical corrosion kinetics would have a LI equal to 1, with no presence on any localized corrosion [25, 42]. When a system behave ideally, the average of the current noise signal is equal or close to zero, which leads to  $S_I \approx rms(I)$  and therefore LI would be equal to 1. It can be concluded that LI should be considered as a measure of the deviation of a system from the assumed ideal behavior [25, 42].

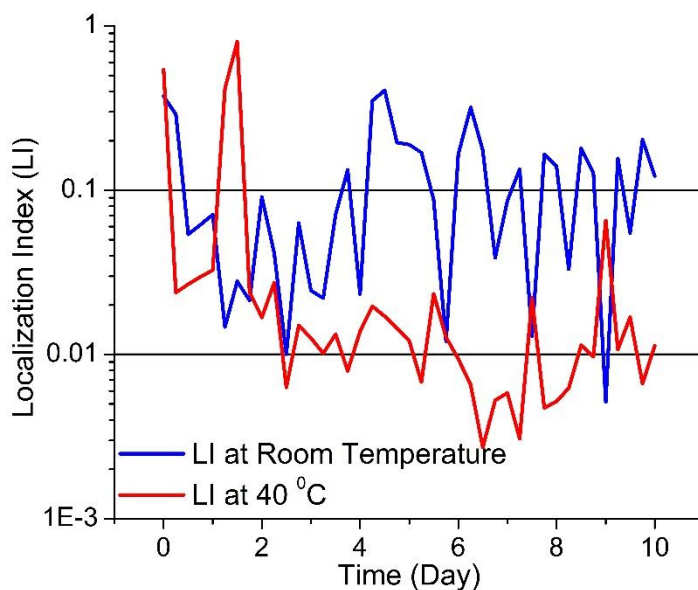


**Figure 7.** Evolution in time of LI at both temperatures for SS-304 exposed to the synthetic seawater.

Figure 7 shows the evolution of the LI at room temperature and at 40 °C. The values of LI at room temperature were higher than the values at 40 °C. There are two possible explanations for this result. The first explanation would be the higher level of pitting corrosion at room temperature, but this is inconsistent because an increase of temperature would accelerate the corrosion processes, under the assumption that the oxygen depletion is not excessive. The second and correct explanation involves a more ideal behavior of the two electrodes used at room temperature, maybe it is more difficult for the two electrodes maintain an identical corrosion kinetics with the increment of temperature, we conclude that the two electrodes used at room temperature behaved more ideally than the two electrodes used at 40 °C, and this conclusion is supported by the SEM micrographs in which there is no presence of pitting corrosion at both temperatures.

#### 4. CONCLUSIONS

a) The Resistance Values ( $R_n$  and  $R_{sn}^0$ ) were very high at both temperatures, indicating very low corrosion rates in the samples, this experimental values agree with the physical observations carried out in the SEM, because the presence of corrosion products was almost negligible after 10 days of immersion.

b) The visual observation of the samples clearly showed more corrosion products at 40 °C, which gives validity to the data obtained with the electrochemical techniques, in which there is a clear difference between the values obtained at 40 °C and the values obtained at Room Temperature.

c) The results obtained with the potentiodynamic polarization curves agree with the results obtained with the electrochemical noise, although it must be say that the average resistance values obtained with the electrochemical noise were greater than the resistance values obtained with the polarization curves.

d) The values of " $R_{sn}^0$ " were higher than the values of " $R_n$ " at the same temperature, so " $R_{sn}^0$ " suggests lower corrosion rates than " $R_n$ ". The values of " $R_{sn}^0$ " and " $R_n$ " are greater at Room Temperature, and this is a confirmation of higher corrosion rates at 40 °C.

e) The values of LI were higher at Room Temperature, indicating the presence of pitting corrosion at this temperature, the absence of pits at both temperatures is a prove against the LI as a reliable index able to detect the presence of pitting corrosion, high values of LI only indicate similar corrosion kinetics between the two electrodes and not a pitting process.

#### References

1. N.B. Hakiki, S. Boudin, B. Rondot and M. Da Cunha Belo, *Corros. Sci.*, 37 (1995) 1809.
2. R.M. Fernández-Domene, R. Sánchez-Tovar, C. Escrivà-Cerdán, R. Leiva-García and J. García-Antón, *Corrosion*, 70 (2014) 390.
3. H. Tsuchiya, S. Fujimoto, O. Chihara and T. Shibata, *Electrochim. Acta*, 47 (2002) 4357.
4. L. Freire, M.J. Carmezim, M.G.S. Ferreira and M.F. Montemor, *Electrochim. Acta*, 55 (2010) 6174.
5. T.L. Sudesh, L. Wijesinghe and D.J. Blackwood, *Appl. Surf. Sci.*, 253 (2006) 1006.

6. M.J. Carmezim, A.M. Simoes, M.F. Montemor and M. Da Cunha Belo, *Corros. Sci.*, 47 (2005) 581.
7. C.-O.A. Olsson and D. Landolt, *Electrochimica Acta*, 48 (2003) 1093.
8. L.P.H. Jeurgens, W.G. Sloof, F.D. Tichelaar and E.J. Mittemeijer, *Phys. Rev. B*, 62 (2000) 4707.
9. R. Franchy, *Surface Science Reports*, 38 (2000) 195.
10. A.J. Davenport, L.J. Oblonsky, M.P. Ryan and M.F. Toney, *J. Electrochem. Soc.*, 147 (2000) 2162.
11. G.S. Frankel, H.S. Isaacs, J.R. Scully and J.D. Sinclair, *Corrosion Science: A Retrospective and Current Status in Honor of Robert P. Frankenthal*, The Electrochemical Society, Inc., (2002) New Jersey, USA.
12. D. Landolt, *Corrosion and Surface Chemistry of Metals*, EPFL Press, (2007) Laussane, Switzerland.
13. E. McCafferty, *Introduction to Corrosion Science*, Springer Science+Business Media, (2010) New York, USA.
14. C. Cuevas-Arteaga, *Revista Mexicana de Ingeniería Química*, 5 (2006) 27.
15. C. Cuevas-Arteaga and J. Porcayo-Calderón, *Materials Science and Engineering*, 435-436 (2006) 439.
16. C. Cuevas-Arteaga, J. Uruchurtu-Chavarín and M.A. Martínez, *Portugaliae Electrochimica Acta*, 23 (2005) 3.
17. A.U. Malik, S. Ahmad, I. Andijani and S. Al-Fouzan, *Desalination*, 123 (1999) 205.
18. L.L. Machuca, S.I. Bailey and R. Gubner, *Corrosion Science*, 64 (2012) 8.
19. ASTM D 1141-98. Standard Practice for the preparation of substitute ocean water.
20. J.M. Sánchez-Amaya, M. Bethencourt, L. González-Rovira y F.J. Botana, *Revista de Metalurgia*, 45 (2009) 143.
21. K. Zakowski, M. Szocinski and M. Narozny, *Anti-Corrosion Methods and Materials*, 60 (2013) 95.
22. J.R. Galvele, *Corrosion Science*, 47 (2005) 3053.
23. J.R. Scully, *Corrosion*, 56 (2000) 199.
24. H.H. Uhlig and R.W. Revie, *Corrosion and Corrosion Control*, Wiley and Sons, (2008) New Jersey, USA.
25. F. Mansfeld, Z. Sun, C.H. Hsu and A. Nagiub, *Corrosion Science*, 43 (2001) 341.
26. C. Cuevas-Arteaga and M.O. Concha-Guzman, *Corrosion Engineering, Science and Technology*, 44 (2009) 57.
27. C. Cuevas-Arteaga, *Corrosion Science*, 50 (2008) 650.
28. C. Cuevas-Arteaga and J. Porcayo-Calderón, *Materials Science and Engineering*, A 435-436 (2006) 439.
29. C. A. Loto, *Int. J. Electrochem. Sci.*, 7 (2012) 9248.
30. U. Bertocci, J. Frydman, C. Gabriele, F. Huet, and M. Keddam, *J Electrochem. Soc.*, 145 (1998) 2780.
31. S. Ritter, F. Huet and R.A. Cottis, *Materials and Corrosion*, 63 (2012) 297.
32. European Cooperative Group on Corrosion Monitoring of Nuclear Plants. <http://www.ecg-comon.org/guideline/PSDcalculator.html> (Accessed June 12, 2016)
33. M. G. Pujar, T. Anita, H. Shaikh, R. K. Dayal and H. S. Khatak, *Int. J. Electrochem. Sci.* 2 (2007) 301.
34. R.A. Cottis, *Corrosion*, 57 (2001) 265.
35. A. Torres, J. Uruchurtu, J.G. González-Rodríguez and S. Serna, *Corrosion*, 63 (2007) 866
36. C.B. Breslin and A.L. Rudd, *Corrosion Science*, 42 (2000) 1023.
37. M. Hernández et al., *Corrosion Science*, 51 (2009) 499.
38. T. Anita et al., *Corrosion Science*, 48 (2006) 2689.
39. A.-M. Lafront et al., *Electrochimica Acta*, 51 (2005) 489.
40. J.M. Sanchez-Amaya et al., *Corrosion Science*, 47 (2005) 3280.

41. D. Cabrera-de la Cruz, R. Galván-Martínez, R. Orozco-Cruz and E. Martínez-Martínez, Corrosión de un Acero Inoxidable AISI 410 en agua de mar bajo condiciones de flujo turbulento mediante la técnica de Ruido Electroquímico, 3rd Meeting of the Mexican Section ECS, Zacatecas, Mexico, 2010, 641.
42. F. Mansfeld and Z. Sun, *Corrosion*, 55(1999) 915.

© 2016 The Authors. Published by ESG ([www.electrochemsci.org](http://www.electrochemsci.org)). This article is an open access article distributed under the terms and conditions of the Creative Commons Attribution license (<http://creativecommons.org/licenses/by/4.0/>).